Small Anechoic Chamber Design Method for On-Line and On-Site Passive Intermodulation Measurement

Zhanghua Cai, *Student Member, IEEE*, Yantao Zhou, Lie Liu, *Senior Member, IEEE*, Yihong Qi, *Senior Member, IEEE*, Wei Yu, *Member, IEEE*, Jun Fan, *Fellow, IEEE*, Ming Yu, *Fellow, IEEE*, and Qingchun Luo, *Member, IEEE*

***Abstract*— A design method is proposed in this article for on-line (online measurement: measurement when producing devices) and on-site (on-site measurement: measurement when using devices) passive intermodulation (PIM) measurement with a small-size anechoic chamber. In a PIM measurement, the role of an anechoic chamber is to shield extraneous electromagnetic signal and reduce reflection, so that an accurate measurement result can be obtained. However, the chamber itself may introduce new PIM sources due to the nonlinearity in absorbing material and shielding enclosure. The traditional method to lower the influence of chamber to PIM measurement is to design a large-size PIM test chamber in order to reduce the PIM level by path loss. In this article, an innovative design concept of the PIM test chamber is presented by controlling the PIM source level of the anechoic chamber instead of increasing the size of the chamber. It can significantly reduce the chamber size using this method, particularly suitable for on-line and on-site PIM measurement. To implement the concept, absorbing material and shielding enclosure structure with extremely low PIM are developed. The design concept includes defining the worst-case reflection level, estimating the PIM level due to reflected signals, and determining the smallest size of the chamber that meets the design specifications. Finally, two PIM test chambers are built to demonstrate the design concept. PIM measurement results are given to verify the theoretical analysis.**

***Index Terms*— Absorbing material, passive intermodulation (PIM), PIM chamber design concept, PIM measurement, PIM source, PIM test chamber, shielding enclosure.**

Manuscript received July 5, 2019; accepted August 13, 2019. Date of publication September 2, 2019; date of current version May 12, 2020. This work was supported by the National Natural Science Foundation of China under Grant 61671203. The Associate Editor coordinating the review process was Leonid Belostotski. *(Corresponding author: Yantao Zhou.)*

Z. Cai and Y. Zhou are with the School of Electrical and Information Engineering, Hunan University, Changsha 410082, China (e-mail: zhanghua.cai@generaltest.com; yantao_z@hnu.edu.cn).

L. Liu and Q. Luo are with the School of Electrical and Information Engineering, Hunan University, Changsha 410082, China, and also with General Test Systems Inc., Shenzhen 518102, China (e-mail: lie.liu@generaltest.com; qingchun.luo@generaltest.com).

Y. Qi is with General Test Systems Inc., Shenzhen 518102, China, with the School of Electrical and Information Engineering, Hunan University, Changsha 410082, China, and also with the EMC Laboratory, Missouri University of Science and Technology, Rolla, MO 65409 USA (e-mail: yihong.qi@generaltest.com).

W. Yu is with General Test Systems Inc., Shenzhen 518104, China (e-mail: fred.yu@generaltest.com).

J. Fan is with the EMC Laboratory, Missouri University of Science and Technology, Rolla, MO 65409 USA (e-mail: jfan@mst.edu).

M. Yu is with the Electronics Engineering Department, The Chinese University of Hong Kong, Hong Kong (e-mail: ming.yu@cuhk.edu.hk).

Color versions of one or more of the figures in this article are available online at http://ieeexplore.ieee.org.

Digital Object Identifier 10.1109/TIM.2019.2937425

I. Introduction

PASSIVE intermodulation (PIM) is an important performance specification for industrial products such as antenna [1], [2], cable [3], connector [4], [5], and other microwave components. When multiple signals with different frequencies are mixed in nonlinear devices, harmonic signals will be generated. If these harmonic signals fall into the passband of receivers, PIM distortion occurs. It degrades the performance of high-sensitivity communication systems and decreases channel capacity, adversely affecting satellite [4], cellular base station [1], [6], and wireless communication system [3]. Driven by emerging technologies such as 5G wireless systems, autonomous vehicles, higher power, and higher receiver sensitivity becomes the trend of a communication system. PIM distortion will then inevitably become more critical [7].

PIM is caused by nonlinear sources in radio-frequency (RF) devices. The nonlinearities have two types: nonlinear contact [4] and nonlinear material [8]. The contact nonlinearities mainly include metal–metal contact and metal–oxide–metal contact [9]. The material nonlinearities refer to the intrinsic nonlinearity of material, such as electrically nonlinear characteristics of ferromagnetic materials [3], [10], piezoelectric effects [11], and electro-thermal effects [12]. The nonlinearities are caused by a variety of physical mechanisms such as electron tunneling [13], microdischarge between microcracks and across voids in metals, electro-thermal effect, thermionic emission effect, and ferromagnetic effect. In many cases, there are multiple concurrent effects that can generate PIM. Thus, the PIM level is hard to predict accurately due to the complexity and uncertainty of influencing factors. Therefore, it is often evaluated by measurement.

The nonlinear RF devices used in communication systems should meet specific PIM targets in the process of production. All devices, which can potentially generate PIM, should be measured. Processing differences exist in all products, which may result in different PIM levels. For example, loose contact of connectors during assembly [14] or a different surface roughness of conductor during processing [15] can result in different PIM levels. Therefore, these products need to be measured one by one. An on-line measurement system for PIM can speed up measurement and improve production efficiency because PIM performance changes with a small change in the structure, such as thin oxide layers or pollution of the

surface, loose contact, and debris at the contact areas [3]. Even the temperature variation would result in the change of PIM level. Thus, the PIM performance of products may be changed in the process of storage and transportation, which may impact the reliability and consistency of wireless communication systems and increase the manufacturing and maintenance costs. Therefore, on-site measurement of PIM is also necessary to ensure that the PIM specification of devices is always maintained at an acceptable level.

As the antenna is an indispensable component of a wireless communication system [16]–[19], the measurement of antenna has always been valued [20]–[24]. Anechoic chamber plays an important role in the radiation characteristics measurement of the antenna [25]–[29] and also in the PIM measurement. The RF energy radiated from antenna under test (AUT) can cause PIM on nearby objects. These PIM signals may transmit to the AUT, resulting in measurement errors. The external RF signals may also interfere with the AUT, resulting in low test quality. By using an anechoic chamber in the PIM measurement, the enclosure of the chamber is used as a shielding structure to eliminate the effects of external RF signals and surrounding objects. In addition, the inner chamber walls are covered with a layer of absorbing material. When electromagnetic waves are incident on the absorbing material layer of the chamber, most of the electromagnetic waves are absorbed, which can provide a simulated free space for the electromagnetic waves ideally.

PIM over common public radio interface (CPRI) testing is a very convenient and inexpensive measurement method without anechoic chamber [30]. However, this method is usually for the on-site inspection of PIM of already installed base station antennas; it is not suitable for general PIM detection during production and transportation. The environment requirements of PIM measurement are very high, and there may be interference sources of various frequencies in the site. The measurement error without the anechoic chamber is very large. If AUT is placed in the air like a base station antenna, the disassembly and assembly of the AUT are very troublesome, which affects the efficiency of the production line measurement. PIM test chamber is desirable for on-line and on-site PIM measurements, as it can provide a standardized testing environment.

However, in reality, an anechoic chamber itself can also produce PIM, due to the nonlinearity in absorbing material and the connection of shielding enclosure [31]. As shown in Fig. 1, there may be five PIM signals that the instrument can detect, where $S_{\mathrm{IM\_Ai}}$ is the PIM generated at the AUT by the input signals S_{f_1} and S_{f_2}, $S_{\mathrm{IM\_Ar}}$ is the PIM generated at the AUT by the reflected signals S'_{f_1} and S'_{f_2}, $S'_{\mathrm{IM\_Ai}}$ is the reflected PIM signal from $S_{\mathrm{IM\_Ai}}$ received by the AUT, and $S_{\mathrm{IM\_AM}}$ and $S_{\mathrm{IM\_SE}}$ are the PIM signals generated at the absorbers and shielding enclosure, respectively, by the radiated signals S_{f_1} and S_{f_2}. Among these five PIM signals, $S_{\mathrm{IM\_Ai}}$ is the only wanted one to be measured. The others are the sources of error. The conventional method to lower the unwanted PIM products is to design a large-size chamber, which can reduce the PIM levels by increasing the path loss. However, the large dimension will result in higher manufacturing cost

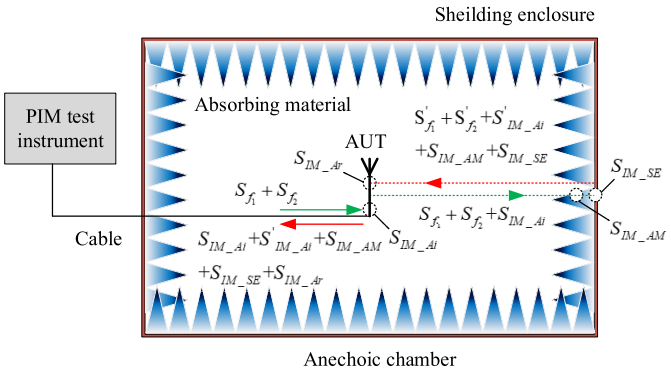

Fig. 1. PIM signals in the test chamber.

and larger real estate. After the chamber is built, it will also be very difficult to move. These issues make the conventional anechoic chamber not suitable for on-line or on-site PIM measurement, where a small-size chamber is preferred due to the requirements for easy assembly and relocation when needed, as well as low cost and high efficiency.

Recent work on PIM measurement mainly focuses on the study of PIM measurement system [32]–[37] and device of PIM tester [38]–[40]. However, as far as we know, there was no systematic theory or method reported concerning the design of PIM test chambers. This article proposes a design concept for a miniature PIM test chamber in order to meet the on-line and on-site PIM measurement requirements. Instead of attenuating the PIM levels using a large physical size of the chamber, first, absorber and shielding enclosure are designed to achieve low levels of PIM. When $S_{\mathrm{IM\_AM}}$ and $S_{\mathrm{IM\_SE}}$ are sufficiently low, the remaining measurement errors are the PIM signals $S_{\mathrm{IM\_Ar}}$ and $S'_{\mathrm{IM\_Ai}}$, which can be attenuated by the absorbers as well as the path loss in the chamber. Since the levels of $S_{\mathrm{IM\_Ar}}$ and $S'_{\mathrm{IM\_Ai}}$ are usually much lower than those of $S_{\mathrm{IM\_AM}}$ and $S_{\mathrm{IM\_SE}}$, the requirement of path loss can be significantly lowered. In other words, the PIM test chamber with a small size can be realized. If the absorption of the absorber can be further increased, the size of the chamber could be further reduced.

This article is organized as follows. Section II introduces the design of absorbing material and shielding enclosure with low PIM. Section III analyzes the measurement error due to reflected signals and provides a feasible design principle of chamber size. Section IV illustrates the measured results. Finally, Section V concludes this article.

II. Low PIM Design Method of PIM Test Chamber

As discussed earlier, our proposed design concept for low PIM test chamber starts with low PIM absorbing material and low PIM shielding enclosure.

A. Absorbing Material

Microwave absorbing materials or microwave absorbers used for anechoic chambers were developed after WWII mainly due to the requirement of radar and antenna measurement. Since the 1960s, the main manufacturers employ similar

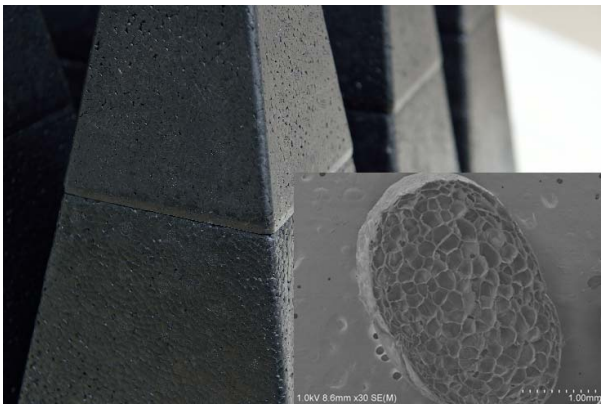

Fig. 2. EPP absorber and SEM morphology of EPP particle.

formula and process to fabricate pyramidal absorber blocks due to relatively simple craftwork and low cost. The raw materials are comprised of polyurethane (PU) foam (usually called sponge) and carbon black (CB) or graphite powder. The handcraft process includes impreg of carbon powder solution and drying with sunlight or inside conviction oven. The simple process may result not only in low fabrication cost but also in nonuniform performance and poor quality. Most importantly, the large-sized carbon particles may contact each other imperfectly to form loose clusters, which are considered to be the main cause of PIM noise.

More recently, a brand-new formula and process with expended polypropylene (EPP in short) or PP foam mixed with CB in nanometer particles were proposed to replace the traditional types of EM wave absorber. As shown in Fig. 2, EPP absorbers prepared with molding process have smooth surfaces and precise dimensions. The intrinsic absorbent is CB particles with an average size of 50 nm instead of large graphite particles in micrometers. The advantages of molding technique include an extremely uniform distribution of absorbent nanoparticles and consistent dielectric properties. As shown in Fig. 2, even in an SEM image, one can hardly see any isolated CB particles, the main cause of PIM noise. As a matter of fact, all of CB particles are well embedded inside PP resin during the mixing with double screw extruder. In summary, EPP absorber can not only provide much better EM performance as compared to the PU-based sponge absorber but also result in extremely low PIM noise due to the uniform dispersion of conductive particles.

In Fig. 3, a piece of pyramid EPP absorber was measured by our in-house free-space measurement system. The measurement results have already been validated with numerical simulation in [41]. It can be clearly seen that the EPP absorber can achieve very low reflectivity in the range of approximately −30 dB from 0.86 to 8 GHz and then lower than −50 dB from 8 to 18 GHz.

The PIM level generated by the EPP absorbers compared with the PU absorbers under the same testing environment will be measured and analyzed in Section IV.

B. Shielding Enclosure

Building an integral, one-piece shielding enclosure for the anechoic chamber is expensive and difficult. Usually, it is

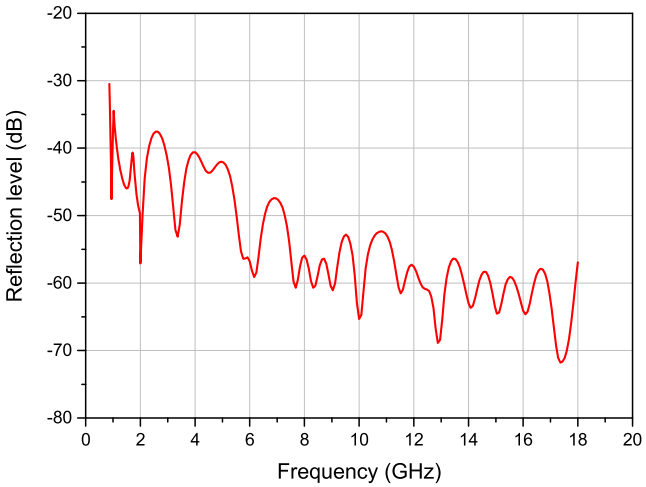

Fig. 3. Measured reflectivity of pyramid EPP absorber with a free-space method.

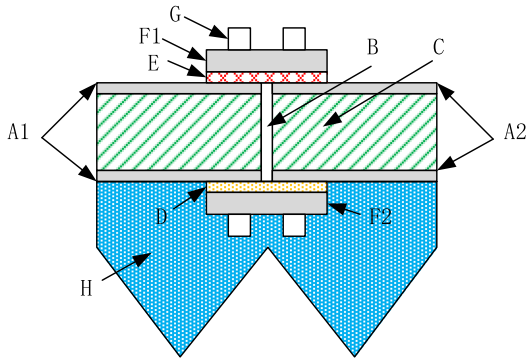

Fig. 4. Splicing structure of shielding enclosure.

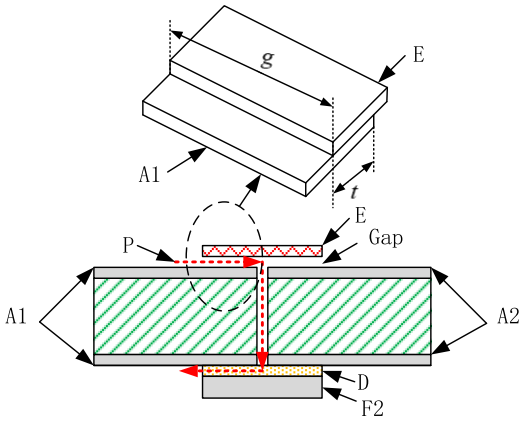

Fig. 5. Propagation path of the electromagnetic wave at gap position.

spliced by several metal plates. The metal–metal contacts can be fixed by welding, screw, or conductive adhesive. However, these conventional joints introduce contact nonlinearity, which can generate PIM. In addition, welding can produce uneven conductive points such as burrs and solder holes. The splicing method using conductive glue or screw can generate a gap in the butt joint and cause electromagnetic wave leakage.

A novel splicing structure of shielding enclosure is shown in Fig. 4 [42], where A1 and A2 are sandwich boards which are made of two nonferromagnetic metal plates with a core layer C

in between; layer C is made of flame retardant materials. Using the sandwich board as shielding enclosure wall can reduce the thickness of the metal and enhance fire resistance. As shown in Fig. 4, the splicing structure connects A1 and A2 in a nonconductive manner. Between them is insulating glue, marked as B in Fig. 4. The inside of the splicing position is covered with elastic nonferromagnetic lossy material (marked as D in Fig. 4), which can absorb electromagnetic waves at both directions. The outside of the splicing position is covered with nonferromagnetic metal (marked as E in Fig. 4) to prevent external electromagnetic waves from entering the gap. The material of E is metal with good elasticity and ductility, which can make it tightly contacted with A1 and A2. The lossy layer D and shielding layer E can enhance the shielding effectiveness at the splicing gap. They are pressed tightly in the splicing position by metal plates marked as F1 and F2 in Fig. 4. F1 and F2 can be fixed on the boards A1 and A2 by rivet or bolt (marked as G in Fig. 4). The inside of shielding enclosure is finally covered with absorbing material (marked as H in Fig. 4).

The first advantage of this structure is a low PIM generation. The metal plates in A1 and A2 are not in direct contact, except on the outside surface between E and A1/A2. Even though this contact may generate PIM, signals arriving at E from the inside are significantly attenuated by the absorber H and lossy layer D. Furthermore, the generated PIM noise is absorbed again by the lossy layer D. The PIM of shielding enclosure is also affected by processing technology, such as the tightness of rivets. This section explains the low PIM characteristics of the proposed structure from a theoretical perspective. The feasibility of the structure will be indirectly validated by the overall performance of the PIM test chamber in Section IV.

At the same time, this structure can achieve good shielding effectiveness. The gaps in the splicing structure are the main factors impacting shielding effectiveness. The dotted line marked as P in Fig. 5 illustrates a path, in which electromagnetic waves could enter the anechoic chamber. The minimum shielding effectiveness at this splicing position can be estimated as follows:

$$\mathrm{SE} = R + A \tag{1}$$

$$R = 20\lg\left[\frac{(1+N)^2}{4N}\right] \tag{2}$$

$$A = 20\lg e^{\pi t/g} = 27.3t/g \tag{3}$$

where R represents the reflection loss, A represents the transmission loss, g represents the length of the gap between E and A1/A2, t represents the depth of the gap between E and A1/A2, as shown in Fig. 5, and N is the ratio of wave impedance at the gap between E and A1/A2 to the free-space wave impedance. For plane wave, N is determined as follows:

$$N = j6.69 \times 10^{-5} fg \tag{4}$$

where f represents the frequency in megahertz (MHz) when g is in centimeter.

The transmission loss increases with the increase of the gap depth t according to (3). Therefore, shielding effectiveness can be improved by increasing the contact width between E and A1/A2. Moreover, the external signals need to pass through two more gaps (between E and A1/A2 and between F2 and A1/A2), which would further increase loss. As a result, an energy that enters the chamber after passing through this splicing structure will be negligible.

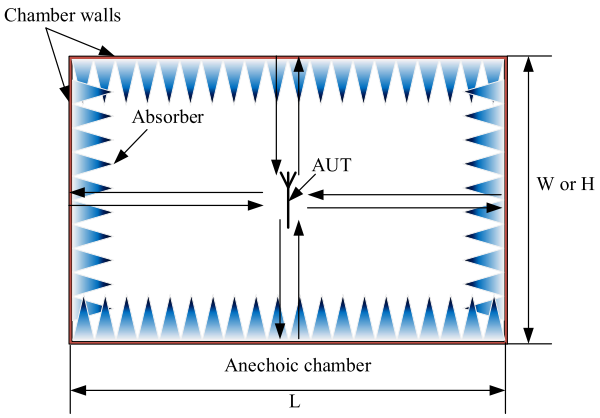

Fig. 6. Main reflected paths in PIM test chamber.

By carefully improving the absorber and shielding enclosure of the anechoic chamber, two sources of error in low PIM measurement can be eliminated or reduced. This makes a small PIM test chamber possible. The size of the chamber will then be determined by the two remaining sources of error in PIM measurement due to reflections, which will be discussed in Section III.

III. Small-Size Design Principle of PIM Test Chamber

A. Reflection Level

When the PIM noise generated at the absorber and shielding enclosure is negligible, the measurement error then becomes dominated by $S_{\mathrm{IM\_Ar}}$ and $S'_{\mathrm{IM\_Ai}}$, which are decided by the reflection level of chamber. As illustrated in Fig. 6, the AUT is located in the center of a rectangular anechoic chamber. Because the absorber does not perfectly absorb, energy can be reflected to the AUT by multiple paths. The more the reflected energy, the higher are the $S_{\mathrm{IM\_Ar}}$ and $S'_{\mathrm{IM\_Ai}}$ levels.

The reflection level of the PIM test chamber can be defined as the ratio of the received power to the transmitted power of AUT. The following calculation method can be used to estimate the worst-case reflection level. Due to the absorbing effect of absorber on the wall, the reflected energy after two or more reflections can be ignored. Only the single reflected energy is considered. The single reflection paths are drawn in Fig. 6. There are totally six of these rays. Two additional paths from the ceiling and floor are not drawn. The fact that the actual signals may be refracted at the absorber surface is ignored. What is also ignored are any phase shifts caused by the propagation velocity in the absorber, which is slower than that in the free space.

The reflection level of each path can be determined using the Friis transmission equation

$$R = \frac{P_{\mathrm{r}}}{P_{\mathrm{t}}} = G_{\mathrm{t}} G_{\mathrm{r}} \left(\frac{\lambda}{4\pi 2d}\right)^2 R_{\mathrm{a}} \tag{5}$$

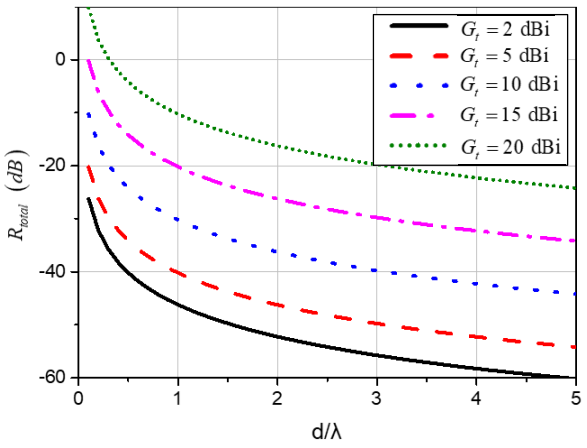

Fig. 7. Reflection level change with distance d.

where P_r and P_t are the received power and transmitted power of AUT, respectively, G_t and G_r are the gain of transmitting antenna and receiving antenna, respectively, λ is the wavelength in free space, d is the distance between AUT and chamber wall, R_a is the reflection coefficient considering the absorber. In this case, both the receiving and transmitting antennas are the AUT. In other words, $G_r = G_t$. Assume that the anechoic chamber is a cube. In this way, we can get a result related to a single distance. Also, assume that all the radiated directions of the AUT have the peak gain in order to estimate a worst-case reflection level of the PIM test chamber. Then, the total reflection level can be expressed as follows:

$$R_{\text{total}} = 6G_t^2 \left(\frac{\lambda}{8\pi d}\right)^2 R_a. \tag{6}$$

Expressed in decibels, the equation is modified as follows:

$$R_{\text{total}}(\text{dB}) = 2G_t(\text{dB}) + 20\lg\left(\frac{\lambda}{8\pi d}\right) + R_a(\text{dB}) + 10\lg 6 \tag{7}$$

where G_t(dB) is in dBi, R_a(dB) is in dB relative to a metal plate, and λ and d are both in meters.

Assume $R_a = -30$ dB, which can be achieved over a wide band according to Fig. 3. The curves in Fig. 7 show the reflection level changing with distance d/λ under different G_t values. In the real world, antenna cannot have the peak gain in all the six directions. In addition, the beamwidth of antenna usually decreases with the increase of the gain. High-gain antenna may have much smaller reflection in other directions comparing with the main radiated direction. Thus, the real reflection level would be lower than the calculated value from (7).

B. Error Analysis and Smallest Design Size

The next step is to estimate the PIM level generated by the reflected energy in order to get an appropriate threshold of reflection level. PIM products occur at frequencies $\pm mf_1 \pm nf_2$, where $m+n$ is the order of PIM products. Even-order products can be ignored because they are always far away from carrier band. The third-order PIM products at frequencies $2f_1 - f_2$ and $2f_2 - f_1$ are closest to the carrier frequency and have the highest level in all the odd-order PIM products.

The third-order PIM is the main distortion in the mobile communication system. PIM measurement usually targets at the third-order PIM. It can be measured more easily because it has higher level than higher order PIM. We can also predict the higher order PIM level by the measured result of the third-order PIM level. Thus, the proposed method determines the reflection level of PIM chamber by estimating the third-order PIM.

A nonlinear device with input x and output y can be described by power series

$$y = \sum_{k=1}^{\infty} a_k x^k \tag{8}$$

where a_k represents the physical properties of nonlinearity, and x and y can be seen as the input and output voltages of the nonlinear device, respectively. The input voltage can be expressed as a sum of two cosine signals with different frequencies as follows:

$$V_{\text{in}} = V_1\cos(\omega_1 t) + V_2\cos(\omega_2 t) \tag{9}$$

where $\omega_i = 2\pi f_i$, and f_i represents the frequency in hertz. Then, the nonlinear output voltage can be written as follows:

$$V_{\text{out}} = \sum_{k=1}^{\infty} a_k (V_1\cos(\omega_1 t) + V_2\cos(\omega_2 t))^k. \tag{10}$$

The third-order PIM components are contained in the third term ($k = 3$) of the power series, which is expanded as the following polynomial:

$$\begin{aligned} & a_3\left[V_1\cos(\omega_1 t) + V_2\cos(\omega_2 t)\right]^3 \\ &= a_3 \left[\begin{array}{l} \dfrac{3V_1}{2}\left(\dfrac{V_1^2}{2} + V_2^2\right)\cos\omega_1 t \\ +\dfrac{3V_2}{2}\left(V_1^2 + \dfrac{V_2^2}{2}\right)\cos\omega_2 t \\ +\dfrac{V_1^3}{4}\cos 3\omega_1 t + \dfrac{V_2^3}{4}\cos 3\omega_2 t \\ +\dfrac{3V_1^2V_2}{4}\cos(2\omega_1 - \omega_2)t \\ +\dfrac{3V_1^2V_2}{4}\cos(2\omega_1 + \omega_2)t + \dfrac{3V_1V_2^2}{4}\cos(2\omega_2 - \omega_1)t \\ +\dfrac{3V_1V_2^2}{4}\cos(2\omega_2 + \omega_1)t \end{array}\right]. \end{aligned} \tag{11}$$

The terms with frequency of $2\omega_1 - \omega_2$ or $2\omega_2 - \omega_1$ are what we care about here. For weak nonlinear system, the following relationship exists between the coefficients:

$$|a_k| \gg |a_{k+1}|. \tag{12}$$

Consequently, although the higher order terms ($k > 3$) of the power series also have contributions to the third-order PIM, we can approximately express the third-order PIM only using

the third term ($k = 3$). Thus, one of the third-order PIM components can be estimated as follows:

$$V_{2\omega_1-\omega_2} \approx a_3 \frac{3V_1^2 V_2}{4} \cos[(2\omega_1 - \omega_2)t]. \tag{13}$$

According to (13), a 1-dB increase of the input power results in a 3-dB increase of the power of the third-order PIM. For actual RF components, this relationship may be different due to the impact of the ignored higher order terms and small change of nonlinear characteristics with the change of input power. Empirically, when the input power increases by 1 dB, the power of the third-order PIM increases by about 1–3 dB [1], [33], [36].

According to the reciprocity theorem of antenna, the transmitting and receiving characteristics of the same antenna are the same. It can be considered that the input power and the reflected power have the same nonlinear response at AUT. Thus, we can estimate the third-order PIM level generated by the reflected energy and power change. In order to define the worst case, we assume that the third-order PIM decreases by 1 dB per dB decrease in power. In this case, the levels of $S_{\text{IM\_Ar}}$ and $S'_{\text{IM\_Ai}}$ are equal. Then, the theoretical measurement error due to reflected signals, denoted by δ(dB), can be determined as follows:

$$\begin{aligned}\delta(\text{dB}) &= 10\lg\frac{P_{S_{\text{IM\_Ar}}} + P_{S'_{\text{IM\_Ai}}} + P_{S_{\text{IM\_Ai}}}}{P_{S_{\text{IM\_Ai}}}} \\ &= 10\lg\left(\frac{2P_{S'_{\text{IM\_Ai}}}}{P_{S_{\text{IM\_Ai}}}} + 1\right)\end{aligned} \tag{14}$$

where $P_{S_{\text{IM\_Ar}}}$, $P_{S'_{\text{IM\_Ai}}}$, and $P_{S_{\text{IM\_Ai}}}$ represent the power of PIM signals $S_{\text{IM\_Ar}}$, $S'_{\text{IM\_Ai}}$, and $S_{\text{IM\_Ai}}$, respectively. Notice that $(P_{S'_{\text{IM\_Ai}}}/P_{S_{\text{IM\_Ai}}})$ is the value of the chamber reflection level. Consequently, the reflection level can be written as follows:

$$R_{\text{total}}(\text{dB}) = 10\lg\frac{10^{\delta(\text{dB})/10} - 1}{2}. \tag{15}$$

Let $\delta(\text{dB}) = 1$ dB, which is a fairly small error in the PIM measurement, then the required reflection level of the PIM test chamber is -9 dB. According to Fig. 7, this reflection level can be easily achieved using appropriate absorbing material. Then, path loss in the chamber does not have to be large. In other words, the size of the chamber can be significantly reduced.

Fig. 8 is a schematic to show the size of the chamber. The length of the chamber is $D + 2d$, where D is the diameter of the test region and d is the distance from the test region to the chamber wall. In addition to the reflection level, there is another size limit of PIM test chamber. When the absorbers are too close to the AUT, they would change the characteristics of the AUT. The measured PIM level of the AUT in this situation is also not correct. Thus, d should meet the following two conditions:

$$d \geq \frac{\lambda}{8\pi \times 10^{(R_{\text{total}}(\text{dB}) - 2G_{\text{t}}(\text{dB}) - R_{\text{a}}(\text{dB}) - 10\lg 6)/20}} \tag{16}$$

and

$$d \geq l_{\text{AM}} + d_{\text{AM\_AN}\,\text{min})}. \tag{17}$$

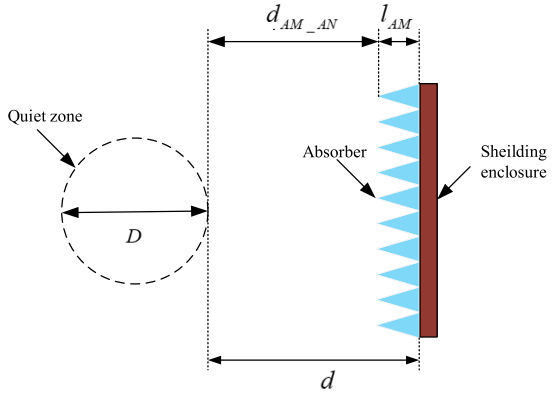

Fig. 8. Size of the PIM test chamber.

Equation (16) is derived from (7) and (15). It defines the limit based on the chamber reflection level for the required PIM measurement error. Equation (17) defines the limit based on the effect of the absorbers on the AUT characteristics, where $d_{\text{AM\_AN(min)}}$ is the minimum distance from the absorbers to the AUT and l_{AM} is the height of the absorbers. $d_{\text{AM\_AN(min)}}$ is related to the performance of the absorbing material. Based on our simulated and measured results, when $d_{\text{AM\_AN}}$ is larger than $\lambda/4$, the impact of the absorbers to the AUT characteristics is relatively small. Moreover, the absorbers can achieve good absorption performance beyond this distance.

In summary, when the maximum wavelength, maximum antenna gain, and requirement for PIM measurement error are given for a specific application, the smallest dimension of the PIM test chamber can be determined using (16) and (17).

IV. Measurement and Analysis

In order to verify the proposed design method of low PIM and small-size PIM test chamber, two PIM test chambers are constructed and analyzed. The first chamber (marked as A) is shown in Fig. 9(a), which is designed using the proposed concept. The absorber and shielding enclosure of chamber A are from those improved designs described in Section II. The external dimensions of chamber A are 3.96 m (L) $\times$ 2.62 m (W) $\times$ 2.6 m (H). The other chamber (marked as B) is illustrated in Fig. 9(b), which is designed using the traditional method. The external dimensions of chamber B are 7 m (L) $\times$ 4 m (W) $\times$ 3.5 m (H). The volume of chamber A is about one-quarter of chamber B. Chamber A is not designed to be smaller considering the size of AUT. For example, the length of the base station antenna is usually greater than 1 m. It needs enough space for placement. But chamber A is still much smaller than the traditional PIM test chamber.

Three experiments were performed to validate the performance of the two chambers. First of all, the PIM level of absorbers is measured. Then, the overall performance of the chambers is evaluated. At last, a measurement for minimum-size verification is done in chamber A. In these experiments, PIM test instruments NTPIMD-900DA (transmitting frequency from 925 to 960 MHz and receiving frequency

Fig. 9. Photograph of two PIM test chambers. (a) PIM test chamber A. (b) PIM test chamber B.

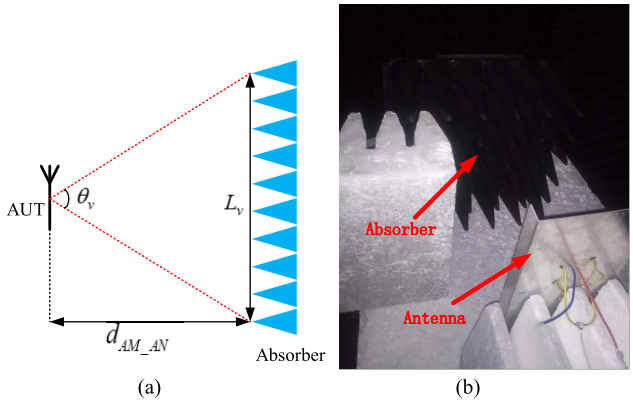

Fig. 10. (a) PIM measurement method of the absorber. (b) Setup of absorber measurement.

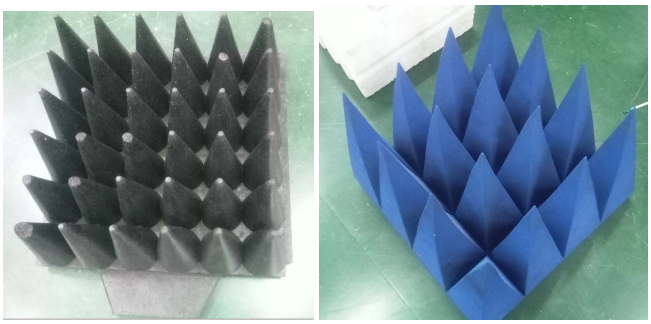

Fig. 11. Photograph of two absorbers. (a) EPP absorber used in PIM test chamber A. (b) Sponge absorber used in PIM test chamber B.

from 880 to 915 MHz) and NTPIMD-1800DA (transmitting frequency from 1805 to 1880 MHz and receiving frequency from 1710 to 1785 MHz) were used, and the input power was set at 43 dBm.

A. Measurement of Absorbers

The test method to evaluate the PIM level of the absorbers is as follows. First, the PIM level of a directional antenna is measured in a PIM test chamber. Then, a block of absorbing material under test was added in the radiation direction of the antenna. The distance between the absorbers and the antenna should not be too close; otherwise, the characteristics of the antenna will be affected. This can be judged by the voltage standing wave ratio (VSWR) of the antenna. If the VSWR does not change with and without the absorbers, it can be considered that the absorbers do not influence the antenna behavior. The appropriate area of the absorbers can be decided by the distance and antenna beamwidth. As illustrated in Fig. 10(a), if θ_v is the vertical half-power beamwidth of the antenna, $d_{\mathrm{AM\_AN}}$ is the distance between the antenna and the absorbers, the vertical length L_{v} of the absorbers can be calculated as follows:

$$L_{\mathrm{v}} = 2d_{\mathrm{AM\_AN}} \tan(\theta_{\mathrm{v}}/2). \tag{18}$$

Similarly, the horizontal length of the absorbers can be calculated as follows:

$$L_{\mathrm{h}} = 2d_{\mathrm{AM\_AN}} \tan(\theta_{\mathrm{h}}/2) \tag{19}$$

where θ_{h} is the horizontal half-power beamwidth of the antenna. Generally, the main radiation energy of the antenna can be considered to concentrate in the 3-dB beamwidth. Thus, the block of the absorbers with an area of $L_{\mathrm{v}} \times L_{\mathrm{h}}$ should receive most of the energies.

When adding the absorbing material, other sources of error in PIM measurement including the PIM generated at the shielding enclosure and the PIM due to the reflection level of the chamber will get attenuated due to the absorption in the absorbing material, while new PIM is generated by the absorbers. As power reduces when the distance increases, the measured PIM generated at the absorbers should also decrease with the increase of the distance. These expectations can help us analyze and understand the results.

Two kinds of absorbers were measured and compared: EPP material [illustrated in Fig. 11(a)] and PU sponge material [illustrated in Fig. 11(b)]. The dimensions of the two absorbers are 600 mm (L) × 600 mm (W) × 290 mm (H) and 600 mm (L) × 600 mm (W) × 500 mm (H), respectively.

The test setup is illustrated in Fig. 10(b). A dual-band directional antenna was used. The lower band is from 800 to 960 MHz with a typical gain of about 10 dBi and a beamwidth of about 55°–65°. The higher band is from 1700 to 2700 MHz with a typical gain of about 9.5 dBi and a beamwidth of about 50°–70°. The size of the antenna is 270 mm (L) × 270 mm (W) × 87.6 mm (H). Throughout the measurement process, the state of the antenna remained unchanged, and the PIM levels when the absorbers were placed at different distances were measured in chamber A.

TABLE I
MEASURED PIM OF AUT UNDER DIFFERENT ABSORBERS

Absorbing material	Measurement distance (mm)	Measured Third-Order PIM (880 to 915 MHz) (dBc)	Measured Third-Order PIM (1710 to 1785 MHz) (dBc)
EPP	50	-169.1	-170.1
	100	-167.6	-170.2
	200	-169.8	-169.7
	300	-168.6	-170.2
PU	50	-124.2	-135.5
	100	-130.5	-141.2
	200	-133.1	-150.5
	300	-140.1	-151.1
AUT without absorber	/	-166.0	-170.7

TABLE II
MEASURED PIM IN DIFFERENT CHAMBERS

PIM test chamber	Measurement distance (mm)	Measured Third-Order PIM (880 to 915 MHz) (dBc)	Measured Third-Order PIM (1710 to 1785 MHz) (dBc)
A	800	-168.2	-170.6
	600	-167.9	-170.4
	400	-168.2	-169.6
	200	-168.3	-172.1
	100	-167.4	-169.9
	50	-167.9	-170.0
B	800	-146.6	-158.9
	600	-143.4	-152.8
	400	-137.1	-151.6
	200	-128.8	-146.8
	100	-123.8	-143.2
	50	-122.5	-139.4

The measured results are shown in Table I. All the measurement distances in this section refer to the distance from the top of the absorbing material to the antenna. Since the measurement setup (such as the connection of connector and cable placement) can affect PIM measurement, it is generally considered that fluctuations within 3 dB are acceptable. All the measured results are averaged values among multiple measurements. It can be seen that the measured PIM results with the EPP absorbers are almost the same at different distances with differences no more than 2.2 dB. They are close to the PIM value without the absorbers. It can, thus, be concluded that the EPP absorber generates extremely low PIM and will not affect the measurement. Other sources of error can also be neglected, especially in the higher band. The phenomenon that the measured PIM is lower with the absorbers than without the absorbers in the lower band is probably caused by the other sources of error because their contribution is attenuated by the absorbers. However, the measured PIM results with the PU sponge absorbers increase significantly compared to the case with the absorbers. The increase comes from PIM generated by the absorbers because the contribution from the other sources of error is attenuated by the absorbers. Furthermore, the PIM level increases as the distance decreases. These results show that the PIM generated at the PU sponge absorbers is much larger (by at least 27.5 dB in the lower band and 18.6 dB in the higher band) and cannot be neglected for the antenna PIM measurement.

B. Measurement of PIM Test Chamber

This experiment is to verify the overall performance of the chambers. In this experiment, the main radiation direction of the antenna was placed toward one side of the chambers, and the distance from the antenna to the sidewall was varied.

The measured results are listed in Table II. The minimum distance between antenna and shielding enclosure in the experiment is 340 mm (the height of absorber plus measuring distance), which is about the wavelength of 880 MHz. For chamber A, there is almost no difference at different distances (variation is less than 3 dB). It can be concluded that chamber A itself does not introduce additional PIM sources (or the generated PIM is small enough) to affect the PIM measurement of the antenna. Indirectly, it validates the effectiveness of the low PIM absorber and shielding enclosure proposed in Section II. However, the PIM level measured in chamber B increases as the distance decreases. Even at a distance of 800 mm, accurate values cannot be measured (deviated from the value of chamber B by more than 10 dB). It indicates that there is PIM generated by chamber B, and thus, path loss in this chamber plays a role in measurement error.

C. Minimum-Size Verification

This experiment is to verify the feasible minimum size proposed in Section III. A directional antenna with a gain of 16 dBi is used to repeat the second experiment in chamber A. The lowest measurement frequency is 880 MHz ($\lambda = 341$ mm), and the reflection level of absorber $R_{\mathrm{a}}(\mathrm{dB})$ at 880 MHz is -33 dB according to Fig. 3. Assume the required chamber reflection level $R_{\mathrm{total}}(\mathrm{dB})$ is less than -9 dB [$\delta(\mathrm{dB}) = 1$ dB]. Then, the d value calculated by (16) is about 83 mm, which is less than a quarter wavelength of operating frequency. If $d_{\mathrm{AM\_AN(min)}}$ is equal to $\lambda/4$, the d value calculated by (17) is 375 mm. Thus, the smallest d of the PIM test chamber should be 375 mm in this example. From here we can see, in many cases, the reflection level has little effect on the measurement, and the minimum size of the chamber depends more on the size of the absorbers.

It is worth mentioning that since the selected antenna is a narrow beam, highly directional antenna, the reflected signal mainly comes from the main radiation direction. Consequently, reducing the distance between the main radiation direction of the antenna and the chamber wall can be equivalent to measuring in a small PIM test chamber.

The measurement results are shown in Table III. It can be seen that the measurement results are consistent at different distances d, even when the distance is less than 375 mm. It can be proved that the minimum size proposed in Section III is feasible. Notice that $d_{\mathrm{AM\_AN(min)}} = \lambda/4$ is a conservatively estimated value. Therefore, accurate values may also be measured within the minimum distance from (17).

In addition, a measurement result outside the chamber is given to show the necessity of PIM test chamber. There is an error of about 26 dB without an anechoic chamber.

TABLE III
MEASURED PIM USING A HIGH-GAIN ANTENNA

PIM test chamber	Measurement distance (mm)	d (mm)	Measured Third-Order PIM (880 to 915 MHz) (dBc)
A	800	1090	-161.1
	600	890	-161.0
	400	690	-161.3
	200	490	-161.3
	100	390	-160.9
	50	340	-160.6
	25	315	-160.8
Outside the chamber	/	/	-134.8

From the three experiments, it can be seen that chamber A, even with a much smaller size than chamber B, does not generate PIM sources to influence measurement results and it can measure accurate PIM values at a shorter distance from the chamber wall. This validates that the proposed concept can be used as a guide to design a small-size chamber for on-line and on-site PIM measurements.

V. CONCLUSION

A design concept of small PIM test chamber is proposed in this article. The proposed method realizes a low PIM measurement environment by controlling the PIM sources at absorbing material and shielding enclosure. With these two main PIM sources addressed, the requirement for path loss in the chamber is significantly reduced. This innovative design concept can significantly reduce the size of the PIM test chamber, particularly suitable for on-line and on-site PIM measurements. Design methodologies for low PIM absorbing material and shielding enclosure are also introduced. The reflection level of the chamber and the PIM level from reflected energy are estimated. The minimum chamber size to meet the given specifications is derived. Finally, the design concept, as well as the improved absorbing material and the proposed splicing structure, was validated by measurements.

REFERENCES

[1] *Passive Intermodulation (PIM) Handling for Base Stations*, document 3GPP TR 37.808, 2013.

[2] D. Wu, Y. Xie, Y. Kuang, and L. Niu, "Prediction of passive intermodulation on mesh reflector antenna using collaborative simulation: Multiscale equivalent method and nonlinear model," *IEEE Trans. Antennas Propaga.*, vol. 66, no. 3, pp. 1516–1521, Mar. 2018.

[3] P. L. Lui, "Passive intermodulation interference in communication systems," *Electron. Commun. Eng. J.*, vol. 2, no. 3, pp. 109–118, Jun. 1990.

[4] X. Chen *et al.*, "Analytic passive intermodulation behavior on the coaxial connector using Monte Carlo approximation," *IEEE Trans. Electromagn. Compat.*, vol. 60, no. 5, pp. 1207–1214, Oct. 2018.

[5] K. Zhang, T. Li, and J. Jiang, "Passive intermodulation of contact nonlinearity on microwave connectors," *IEEE Trans. Electromagn. Compat.*, vol. 60, no. 2, pp. 513–519, Apr. 2018.

[6] J. W. Boyhan, H. F. Henzing, and C. Koduru, "Satellite passive intermodulation: Systems considerations," *IEEE Trans. Aerosp. Electron. Syst.*, vol. 32, no. 3, pp. 1058–1064, Jul. 1996.

[7] R. Butler, "PIM testing: Advanced wireless services emphasize the need for better PIM control," COMMSCOPE, Hickory, NC, USA, White Paper WP-107482-EN (2/14), 2014.

[8] X. Chen and Y. He, "Reconfigurable passive intermodulation behavior on nickel-coated cell array," *IEEE Trans. Electromagn. Compat.*, vol. 59, no. 4, pp. 1027–1034, Aug. 2017.

[9] C. Vicente and H. L. Hartagel, "Passive-intermodulation analysis between rough rectangular waveguide flanges," *IEEE Trans. Microw. Theory Techn.*, vol. 53, no. 8, pp. 2515–2525, Aug. 2005.

[10] G. C. Bailey and A. C. Ehrlich, "A study of RF nonlinearities in nickel," *J. Appl. Phys.*, vol. 50, no. 1, pp. 453–461, Jan. 1979.

[11] J. R. Wilkerson, "Passive intermodulation distortion in radio frequency communication systems," Ph.D. dissertation, North Carolina State Univ., Rayleigh, NC, USA, 2010, pp. 157–160.

[12] J. R. Wilkerson, K. G. Gard, A. G. Schuchinsky, and M. B. Steer, "Electro-thermal theory of intermodulation distortion in lossy microwave components," *IEEE Trans. Microw. Theory Techn.*, vol. 56, no. 12, pp. 2717–2725, Dec. 2008.

[13] J. Russer, A. Ramachandran, A. Cangellaris, and P. Russer, "Phenomenological modeling of passive intermodulation (PIM) due to electron tunneling at metallic contacts," in *IEEE MTT-S Int. Microw. Symp. Dig.*, Jun. 2006, pp. 1129–1132.

[14] H. Yang, H. Wen, Y. Qi, and J. Fan, "An equivalent circuit model to analyze passive intermodulation of loose contact coaxial connectors," *IEEE Trans. Electromagn. Compat.*, vol. 60, no. 5, pp. 1180–1189, Oct. 2018.

[15] P. Ansuinelli, A. G. Schuchinsky, F. Frezza, and M. B. Steer, "Passive intermodulation due to conductor surface roughness," *IEEE Trans. Microw. Theory Techn.*, vol. 66, no. 2, pp. 688–699, Feb. 2018.

[16] M. J. Horst, M. T. Ghasr, and R. Zoughi, "Design of a compact V-band transceiver and antenna for millimeter-wave imaging systems," *IEEE Trans. Instrum. Meas.*, to be published.

[17] Z. Lu, J. Nie, F. Chen, H. Chen, and G. Ou, "Adaptive time taps of STAP under channel mismatch for GNSS antenna arrays," *IEEE Trans. Instrum. Meas.*, vol. 66, no. 11, pp. 2813–2824, Nov. 2017.

[18] A. Buffi, A. Michel, P. Nepa, and B. Tellini, "RSSI measurements for RFID tag classification in smart storage systems," *IEEE Trans. Instrum. Meas.*, vol. 67, no. 4, pp. 894–904, Apr. 2018.

[19] X. Yi, J. Zhang, B. Tian, and C. Jiang, "Design of magnetic resonance sounding antenna and matching circuit for the risk detection of tunnel water-induced disasters," *IEEE Trans. Instrum. Meas.*, to be published.

[20] A. Jam and K. Sarabandi, "A submillimeter-wave near-field measurement setup for on-wafer pattern and gain characterization of antennas and arrays," *IEEE Trans. Instrum. Meas.*, vol. 66, no. 4, pp. 802–811, Apr. 2017.

[21] M. Heikkilä *et al.*, "Field measurement for antenna configuration comparison in challenging NLOS locations," *IEEE Trans. Instrum. Meas.*, vol. 67, no. 10, pp. 2476–2486, Oct. 2018.

[22] N. Decarli and D. Dardari, "Time domain measurements of signals backscattered by wideband RFID tags," *IEEE Trans. Instrum. Meas.*, vol. 67, no. 11, pp. 2548–2560, Nov. 2018.

[23] J. Zheng, J. Ala-Laurinaho, and A. V. Räisänen, "On the one-antenna gain measurement method in probe station environment at mm-wave frequencies," *IEEE Trans. Instrum. Meas.*, to be published.

[24] S. Caban, M. Lerch, S. Pratschner, E. Zöchmann, P. Svoboda, and M. Rupp, "Design of experiments to compare base station antenna configurations," *IEEE Trans. Instrum. Meas.*, to be published.

[25] M. A. Salas-Natera, R. M. Rodriguez-Osorio, and L. de Haro, "Procedure for measurement, characterization, and calibration of active antenna arrays," *IEEE Trans. Instrum. Meas.*, vol. 62, no. 2, pp. 377–391, Feb. 2013.

[26] R. D. Leo and V. M. Primiani, "Radiated immunity tests: Reverberation chamber versus anechoic chamber results," *IEEE Trans. Instrum. Meas.*, vol. 55, no. 4, pp. 1169–1174, Aug. 2006.

[27] A. Cataldo, G. Monti, E. D. Benedetto, G. Cannazza, L. Tarricone, and L. Catarinucci, "Assessment of a TD-based method for characterization of antennas," *IEEE Trans. Instrum. Meas.*, vol. 58, no. 5, pp. 1412–1419, May 2009.

[28] S. Matsukawa, S. Kurokawa, and M. Hirose, "Uncertainty analysis of far-field gain measurement of drgh using the single-antenna method and amplitude center distance," *IEEE Trans. Instrum. Meas.*, to be published.

[29] T. B. Hansen *et al.*, "Methods for locating stray-signal sources in anechoic chambers," *IEEE Trans. Instrum. Meas.*, vol. 57, no. 3, pp. 480–489, Mar. 2008.

[30] R. Fridolfing, "Multi-function CPRI and RF PIM site analyzer," *Microw. J.*, to be published.

[31] Z. Cai *et al.*, "A measurement method for passive intermodulation chamber performance evaluation," *IEEE Trans. Electromagn. Compat.*, vol. 60, no. 5, pp. 1279–1287, Oct. 2018.

[32] J. R. Wilkerson, J. Gard, and M. B. Steer, "Automated broadband high-dynamic-range nonlinear distortion measurement system," *IEEE Trans. Microw. Theory Techn.*, vol. 58, no. 5, pp. 1273–1282, May 2010.
[33] S. Yang, W. Wu, S. Xu, Y.-J. Zhang, D. Stutts, and D. J. Pommerenke, "A passive intermodulation source identification measurement system using a vibration modulation method," *IEEE Trans. Electromagn. Compat.*, vol. 59, no. 6, pp. 1677–1684, Dec. 2017.
[34] A. J. Christianson, J. J. Henrie, and W. J. Chappell, "Higher order intermodulation product measurement of passive components," *IEEE Trans. Microw. Theory Techn.*, vol. 56, no. 7, pp. 1729–1736, Jul. 2008.
[35] F. Abbas, "Measurements of passive intermodulation in 2G and 3G," in *Proc. Eur. IEEE Microw. Conf.*, Sep. 2002, pp. 1–4.
[36] V. Golikov, S. Hienonen, and P. Vainikainen, "Passive intermodulation distortion measurements in mobile communication antennas," in *Proc. IEEE Veh. Technol. Conf. Fall*, vol. 4, Oct. 2001, pp. 2623–2625.
[37] D. Smacchia *et al.*, "Advanced compact setups for passive intermodulation measurements of satellite hardware," *IEEE Trans. Microw. Theory Techn.*, vol. 66, no. 2, pp. 700–710, Feb. 2018.
[38] C. Shi and E. Sánchez-Sinencio, "On-chip two-tone synthesizer based on a mixing-FIR architecture," *IEEE J. Solid-State Circuits*, vol. 52, no. 8, pp. 2105–2116, Aug. 2017.
[39] X. Chen, Y. He, and W. Cui, "Broadband dual-port intermodulation generator for passive intermodulation measurements," *IEEE Microw. Wireless Compon. Lett.*, vol. 27, no. 5, pp. 518–520, May 2017.
[40] P. Soto *et al.*, "Design of advanced waveguide filters for passive intermodulation measurement setups," in *Proc. IEEE MTT-S Int. Conf. Numer. Electromagn. Multiphys. Modeling Optim. RF, Microw., THz. Appl. (NEMO)*, Seville, Spain, May 2017, pp. 335–337.
[41] Y. Zhang, Q. Luo, Y. Zhu, and L. Liu, "Development of conductive expended polypropylene rigid foam for OTA test chamber," *Saf. EMC*, to be published.
[42] L. Liu, H. Xie, W. Yu, and Y. Qi, "Microwave anechoic chamber and shielding case assembly structure thereof," (in Chinese), Chinese Patent 105 386 630 A, 2015.

Zhanghua Cai (S'17) received the B.S. degree in electronic science and technology from Hunan University, Changsha, China, in 2014, where he is currently pursuing the M.S. degree in electronics.

His current research interests include the design of antennas and the design of antenna test systems and theory.

Yantao Zhou received the Ph.D. degree in information and electrical engineering from the Wuhan Naval University of Engineering, Wuhan, China, in 2009.

He is currently a Professor of electric and information engineering with Hunan University, Changsha, China. His current research interests include parallel computing and distributed data management.

Lie Liu (M'09–SM'12) received the B.Sc. degree from the Beijing University of Aeronautics and Astronautics (BUAA), Beijing, China, in 1991, the M.Sc. degree from the China Academy of Launch Vehicle Technology (CALT), Beijing, in 1994, and the Ph.D. degree from Nanyang Technological University, Singapore, in 2003.

From 2002 to 2012, he was a Senior Research Scientist with the Advanced Materials Group of Temasek Laboratories, National University of Singapore, Singapore. Since 2015, he has been a Chief Technical Officer of General Test Systems Inc., Shenzhen, China. He is currently an Adjunct Professor with Hunan University, Changsha, China. He has authored more than 50 papers in journals and conferences and one book chapter. His current research interests include electromagnetic (EM) materials, over-the-air (OTA) measurement of wireless communication systems, and anechoic chamber design.

Yihong Qi (M'92–SM'11) received the B.S. degree in electronics from the National University of Defense Technologies, Changsha, China, in 1982, the M.S. degree in electronics from the Chinese Academy of Space Technology, Beijing, China, in 1985, and the Ph.D. degree in electronics from Xidian University, Xi'an, China, in 1989.

From 1989 to 1993, he was a Post-Doctoral Fellow and then an Associate Professor with Southeast University, Nanjing, China. From 1993 to 1995, he was a Post-Doctoral Researcher with McMaster University, Hamilton, ON, Canada. From 1995 to 2010, he was with Research in Motion (Blackberry), Waterloo, ON, where he was the Director of advanced electromagnetic research. He is currently the President and the Chief Scientist with General Test Systems Inc., Shenzhen, China. He founded DBJay, Zhuhai, China, in 2011, and he is the CTO of ENICE, Nanjing. He is also an Adjunct Professor with the EMC Laboratory, Missouri University of Science and Technology, Rolla, MO, USA, and with Hunan University, Changsha. He holds more than 280 published and pending patents. The patent that of multi-resonance antenna has been used by more than 1.4 billion smartphones annually. The O-ring connector invention is shipping more than 4 billion pieces per year. He is the Contributor of 3GPP and CTIA standards.

Dr. Qi is a Fellow of the Canadian Academy of Engineering. He received the 2017 Technology Achievement Award from the IEEE EMC Society. He was a Distinguished Lecturer of the IEEE EMC Society in 2014 and 2015. He currently serves as the Chairman of the IEEE EMC TC-12. He is a member of the Advisory Board and an Associate Editor of the IEEE TRANSACTIONS ON ELECTROMAGNETIC COMPATIBILITY.

Wei Yu (M'13) received the B.S. degree in electrical engineering from Xi'an Jiaotong University, Xi'an, China, in 1991, the M.S. degree in electrical engineering from the China Academy of Space Technology, Beijing, China, in 1994, and the Ph.D. degree in electrical engineering from Xidian University, Xi'an, in 2000.

From 2001 to 2003, he was a Post-Doctoral Fellow with the University of Waterloo, Waterloo, ON, Canada. He was a CTO with Sunway Communications Ltd., Shenzhen, China, from 2008 to 2012. He founded Antennovation Electronics Inc., Shenzhen, in 2004, and cofounded General Test Systems Inc., Shenzhen, China, in 2012. He is currently a COO with DBJ Technologies, Zhuhai, China, and also the CEO of General Test Systems Inc., Shenzhen. He holds 32 published and pending patents. His current research interests include signal processing and mobile device test system.

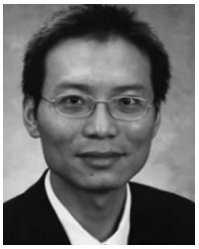

Jun Fan (S'97–M'00–SM'06–F'16) received the B.S. and M.S. degrees in electrical engineering from Tsinghua University, Beijing, China, in 1994 and 1997, respectively, and the Ph.D. degree in electrical engineering from the University of Missouri, Rolla, MO, USA, in 2000.

From 2000 to 2007, he was a Consultant Engineer with NCR Corporation, San Diego, CA, USA. In July 2007, he joined the Missouri University of Science and Technology (formerly University of Missouri), where he is currently an Associate Professor with the Missouri S&T EMC Laboratory. His current research interests include signal integrity and electromagnetic interference (EMI) design in high-speed digital systems, dc power-bus modeling, intrasystem EMI and RF interference, printed circuit board noise reduction, differential signaling, and cable/connector designs.

Dr. Fan was a recipient of the IEEE EMC Society Technical Achievement Award in August 2009. He was the Chair of the IEEE EMC Society TC-9 Computational Electromagnetics Committee from 2006 to 2008 and was a Distinguished Lecturer of the IEEE EMC Society in 2007 and 2008. He is currently the Vice-Chair of the Technical Advisory Committee of the IEEE EMC Society and is an Associate Editor of the IEEE TRANSACTIONS ON ELECTROMAGNETIC COMPATIBILITY and the *EMC Magazine*.

Ming Yu (S'90–M'93–SM'01–F'09) received the Ph.D. degree in electrical engineering from the University of Victoria, Victoria, BC, Canada, in 1995.

In 1993, he joined COM DEV, Cambridge, ON, Canada, as a Technical Staff Member, while finishing his Ph.D. part-time. He was involved in designing passive microwave/RF hardware for both space and ground-based applications. He was a Principal Developer of a variety of COM DEV's core design and tuning software for microwave filters and multiplexers, including computer-aided tuning software in 1994, and a fully automated robotic diplexer tuning system in 1999. He was the Manager of the Filter/Multiplexer Technology (Space Group) and a Staff Scientist of the Corporate Research and Development, COM DEV. In 2003, he demonstrated the world's first robotic filter/diplexer tuning system at the IEEE IMS Conference Workshop in Philadelphia, PA, USA. Until 2016, he was the Chief Scientist and the Director of Research and Development at COM DEV. He was responsible for overseeing the development of the company's research and development roadmap and next-generation products and technologies, including high-frequency and high-power engineering, electromagnetic-based computer-aided design (CAD) and tuning for complex and large problems, and novel miniaturization techniques for microwave networks. He is also an Adjunct Professor with the University of Waterloo (UW), Waterloo, ON, Canada. After COM DEV was acquired by Honeywell, Morristown, NJ, USA, in 2016, he has led the Advanced Technology Group, Cambridge, ON, USA, as the Chief Scientist and a Senior Engineering Fellow. After 24 years in industry full-time and 15 years as an Adjunct Professor at Waterloo, Canada, he joined Electronics Engineering Department, The Chinese University of Hong Kong (CUHK), Hong Kong, as a tenured Full Professor in October 2017. He has authored or coauthored over 150 publications and 30 patents worldwide. He has served as a keynote or invited speaker and session chair for many international conferences and workshops.

Prof. Yu is a fellow of the Canadian Academy of Engineering. He holds the NSERC Discovery Grant (2004–2021) with Waterloo and GRF Grant with CUHK. He was a recipient of the 1995 and 2006 COM DEV Achievement Award for the development of computer-aided tuning algorithms and systems for microwave filters and multiplexers. He was an IEEE Distinguished Microwave Lecturer from 2010 to 2012. He has served as the MTT Filter Committee Chair (MTT-8) and also as the Chair of TPC-11 multiple times. He was an Associate Editor of the IEEE TRANSACTIONS ON MICROWAVE THEORY AND TECHNIQUES.

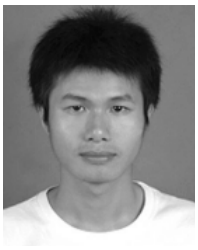

Qingchun Luo (M'16) received the B.S. degree in mathematics and the M.S. degree in electromagnetic from Sichuan University, Chengdu, China, in 2010 and 2013, respectively.

He was engaged in the research of ferrite devices with the CETC 9th Institute, Mianyang, China, in 2013. Since 2014, he has been with General Test Systems Inc., Shenzhen, China, where he devoted in the field of wireless communication measurement (OTA).